To be submitted to The Astrophysical Journal. Version 1.13
Preprint typeset using LaTeX style emulateapj v. 08/22/09

FLASH MIXING ON THE WHITE DWARF COOLING CURVE: SPECTROSCOPIC CONFIRMATION IN NGC 2808[1]

Thomas M. Brown[2], Thierry Lanz[3], Allen V. Sweigart[4], Misty Cracraft[2], Ivan Hubeny[5], and Wayne B. Landsman[6]

To be submitted to The Astrophysical Journal. Version 1.13

ABSTRACT

We present new *HST* far-UV spectroscopy of two dozen hot evolved stars in NGC 2808, a massive globular cluster with a large population of "blue-hook" stars. The blue-hook stars are found in ultraviolet color-magnitude diagrams of the most massive globular clusters, where they fall at luminosities immediately below the hot end of the horizontal branch (HB), in a region of the HR diagram unexplained by canonical stellar evolution theory. Using new theoretical evolutionary and atmospheric models, we have shown that these subluminous HB stars are very likely the progeny of stars that undergo extensive internal mixing during a late He-core flash on the white dwarf cooling curve. This flash mixing leads to hotter temperatures and an enormous enhancement of the surface He and C abundances; the hotter temperatures and associated decrease in the hydrogen opacity shortward of the Lyman limit makes the stars brighter in the extreme UV but appear subluminous in the UV and optical. Our far-UV spectroscopy demonstrates that, relative to normal HB stars at the same color, the blue-hook stars of NGC 2808 are hotter and greatly enhanced in He and C, thus providing unambiguous evidence of flash mixing in the subluminous population. Although the C abundance in the blue-hook stars is orders of magnitude larger than that in the normal HB stars, the atmospheric C abundance in both the blue-hook and normal HB stars appears to be affected by gravitational settling. The abundance variations seen in C, Si, and the Fe-peak elements indicate that atmospheric diffusion is at play in our sample, with all of our hot subdwarfs at 25,000 K to 50,000 K exhibiting large enhancements of the iron-peak elements. The hottest subdwarfs in our blue-hook sample may be pulsators, given that they fall in the temperature range of newly-discovered pulsating subdwarfs in ω Cen.

Subject headings: globular clusters: individual (NGC 2808) – stars: atmospheres – stars: evolution – stars: horizontal branch – ultraviolet: stars

1. INTRODUCTION

For decades, globular clusters have served as the fundamental laboratory for the study of stellar evolution. Their utility arose from the assumption that, within observational errors, each globular cluster appeared to be comprised of stars with a single age and chemical composition. The subsequent discovery that some globular clusters host multiple stellar generations is one of the most exciting developments in the study of resolved stellar populations. These multiple generations were revealed in the color-magnitude diagrams (CMDs) of the most massive globular clusters; examples include the double main sequence (MS) in ω Cen (Anderson 1997) and the triple MS in NGC 2808 (D'Antona et al. 2005; Piotto et al. 2007). The splitting of the MS in these clusters is thought to be due to the presence of subpopulations having He abundances as high as $Y \sim 0.4$ (Piotto et al. 2005), with these He-rich stars being born from the He-rich ejecta of the initial stellar generation.

The existence of these He-rich subpopulations offers the opportunity to test theories of stellar evolution in a new regime, both in the early evolution on the MS and in the late stages beyond. For example, the CMDs of massive clusters exhibit unusual characteristics on the horizontal branch (HB). Regardless of metallicity, massive clusters tend to host significant populations of extreme HB (EHB) stars at $T_{\rm eff} > 20,000$ K. These EHB stars have extremely thin envelopes ($\sim 10^{-3}$-10^{-2} $M_\odot$) – the result of extensive mass loss on the red-giant branch (RGB). The analogs of the EHB stars in the field are the subdwarf B (sdB) stars, which produce the "UV upturn" in the otherwise cool spectra of elliptical galaxies (Brown et al. 1997; Brown et al. 2008). In general, the HB of a high-metallicity cluster will be dominated by red clump stars, while the HB of a low-metallicity cluster will extend to hotter stars, although other parameters (such as age, He abundance, and cluster central density) can play a role in determining the HB morphology (e.g., Gratton et al. 2010; Dotter et al. 2010). At a fixed cluster age, the MS turnoff mass decreases strongly with increasing He abundance, leading to a bluer HB morphology for a given range of RGB mass loss (D'Antona et al. 2002). Because massive clusters are more likely to retain the He-rich ejecta from the initial burst of star formation, He enrichment may explain the HB morphology in those massive clusters that are metal-rich. For example, in NGC 6388 and NGC 6441, the HB extends to hot temperatures, and slopes upward in luminosity at increasing temperature (Rich et al. 1997; Busso et al. 2007). A similar upward slope in the HB morphology of NGC 2808 can be explained by an increasing He abundance (from $0.24 < Y < 0.4$) at increasing temperature (Dalessandro et al. 2011). In this scenario, the EHB stars would be the progeny of the most He-rich MS stars.

Another curiosity in massive clusters is the luminosity dispersion of their EHB stars. In seven massive globular clusters hosting EHB stars, ultraviolet photometry shows that the EHB terminates in a "blue hook" of subluminous stars lying up to

[1] Based on observations made with the NASA/ESA *Hubble Space Telescope*, obtained at STScI, which is operated by AURA, Inc., under NASA contract NAS 5-26555.

[2] Space Telescope Science Institute, 3700 San Martin Drive, Baltimore, MD 21218; tbrown@stsci.edu, cracraft@stsci.edu

[3] Department of Astronomy, University of Maryland, College Park, MD 20742; lanz@astro.umd.edu

[4] Code 667, NASA Goddard Space Flight Center, Greenbelt, MD 20771; allen.v.sweigart@nasa.gov

[5] Steward Observatory, University of Arizona, Tucson, AZ 85712; hubeny@aegis.as.arizona.edu

[6] Adnet Systems, NASA Goddard Space Flight Center, Greenbelt, MD 20771; wayne.b.landsman@nasa.gov

$\sim$1 mag below the canonical HB (D'Cruz et al. 2000; Brown et al. 2001; Brown et al. 2010). The most likely explanation for these stars is a delayed He-core flash. If the RGB mass loss is large enough, a star can evolve off the RGB and undergo a delayed He-core flash either as it crosses the HR diagram ("early hot flasher") or as it descends the white dwarf cooling curve ("late hot flasher") (Castellani & Castellani 1993; D'Cruz et al. 1996). Normally the flash convection does not penetrate into the envelope, due to the high entropy barrier of the strong H-burning shell. However, such penetration is inevitable if He ignites on the white dwarf cooling curve, where the H-burning shell is much weaker. Sweigart (1997) first demonstrated that a flash on the white dwarf cooling curve will mix the hydrogen-rich envelope into the stellar interior, thereby greatly enhancing the surface He, C and possibly N abundances. This result was subsequently confirmed by detailed calculations of the flash-mixing phase by Cassisi et al. (2003) and Miller Bertolami et al. (2008). Brown et al. (2010) demonstrated that flash mixing is the only known mechanism that can plausibly produce the low luminosities of the blue-hook (BH) stars in massive clusters. An independent analysis of optical and UV photometry in NGC 2808 reaffirmed this conclusion (Dalessandro et al. 2011). The low ultraviolet and optical luminosities of the flash-mixed stars are primarily due to their higher effective temperatures (which increases the bolometric correction) and the reduction in their hydrogen opacity below the Lyman limit (which increases the flux emitted in the extreme ultraviolet at the expense of the flux at longer wavelengths).

A key prediction of the flash mixing scenario is a substantial increase in the surface He and C abundances of the BH stars. Spectroscopic evidence in support of this prediction has been found in both field He-sdB stars and hot HB stars in ω Cen. In the field, Lanz et al. (2004) demonstrated that two of three He-rich sdB stars exhibited incredibly strong C lines, implying an atmosphere of 1–2% C by mass. In ω Cen, Moehler et al. (2011) obtained optical spectroscopy of potential BH stars by selecting targets from the faint end of the hot HB tail in an optical CMD of the cluster. They found that all of the HB stars cooler than 30,000 K were He-poor, while nearly three-fourths of the hotter stars had solar to super-solar He abundances, as well as C abundances up to $\sim$4% by mass. Moreover, these C abundances were strongly correlated with the He abundance.

Here, we present recent UV spectroscopy of both normal and subluminous EHB stars in NGC 2808, where the classification comes from high-precision UV photometry. Our objective is to test the flash-mixing scenario by determining the He and C abundances in the BH stars relative to the abundances in the normal EHB stars. In total, spectra were obtained for seven normal EHB stars and eight BH stars. The sample of subluminous stars includes two stars that have luminosities consistent with other BH stars but colors significantly redder than the rest of the BH population, and indeed far redder than expected from flash mixing. We also obtained spectra of five blue HB (BHB) stars, and three unclassified objects with unusually blue UV colors. Finally, our spectroscopy includes a bight post-HB star too hot to ascend the asymptotic giant branch (AGB); such stars are usually classified as AGB-Manqué (AGBM) stars.

2. OBSERVATIONS AND DATA REDUCTION

We obtained spatially-resolved spectra along three slit positions in the center of NGC 2808 using the Space Telescope Imaging Spectrograph (STIS) on the *Hubble Space Telescope (HST)*. The program was originally awarded time in 2004, but was withdrawn before any observations were obtained due to the failure of a STIS power supply later that year. The program was re-proposed and re-awarded time in 2008, but due to scheduling constraints, the observations were delayed until September 2010 (one slit position) and February 2011 (two additional slit positions). The spectra were obtained with the G140L grating, which provides a resolution of $\sim$300 km s^{-1}, although the spectral purity was degraded slightly by our use of the wide $52 \times 2''$ slit. We chose this wide slit in order to maximize the number of hot stars that could be placed within the slit for a given pointing. The NGC 2808 core is far less crowded in the far-UV than in the optical, and so we were able to obtain clean spectra of 24 hot stars using just three slit positions (Figure 1). These sources sample various evolutionary stages in the UV CMD of NGC 2808 (Figure 2).

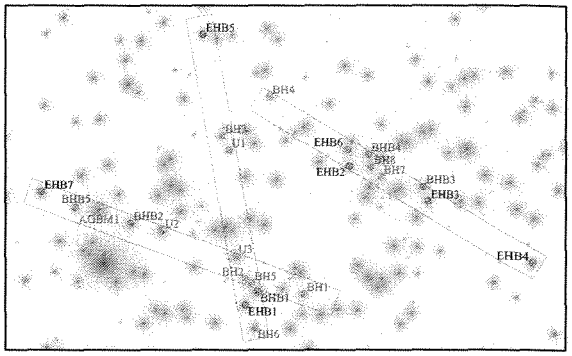

Figure 1. A far-UV image of NGC 2808 (Brown et al. 2001), shown at a logarithmic stretch, with the three spectroscopic slit positions indicated (boxes). Although the slit has dimensions of $52'' \times 2''$, the far-UV detector is only $25''$ across, so we show the slit truncated by the detector. The sources with clean spectroscopy are labeled according to their evolutionary stage: extreme horizontal branch (EHB), blue hook (BH), blue horizontal branch (BHB), AGB-Manqué (AGBM), and unclassified (U). The positions of these stars in the UV CMD of NGC 2808 are shown in Figure 2.

Each of the three slit positions was observed for 5 orbits, with two exposures per orbit, giving a total exposure time ranging from 14442 sec to 14460 sec per slit position and a signal-to-noise ratio (SNR) of $\sim$20 per resolution element. The resolution and SNR were intended to discriminate between stars that have and have not undergone flash mixing, given the enormous differences in atmospheric abundances between these two possibilities. For a given slit position, the individual exposures were dithered by a few pixels along the slit, in order to mitigate detector artifacts and flat-field variations. Because we obtained spectra of multiple stars per slit position, our targets are offset from the slit midline in the dispersion direction. To correctly align in wavelength the sensitivity curve and the counts spectrum of each star, we measured the position within the slit for each star, both in the dispersion and cross-dispersion directions. This alignment was an iterative process. Our initial position estimates used brief (2 sec) CCD images of the cluster obtained through the $52'' \times 2''$ slit at the start of each observing visit, inspected in conjunction with the far-UV and near-UV images of Brown et al. (2001). We then extracted the spectra using the IRAF X1D package, measured the wavelengths of strong interstellar lines, and tweaked the position of each star in the dispersion direction.

By default, the X1D package estimates the gross source counts from an extraction box centered on the object in ques-

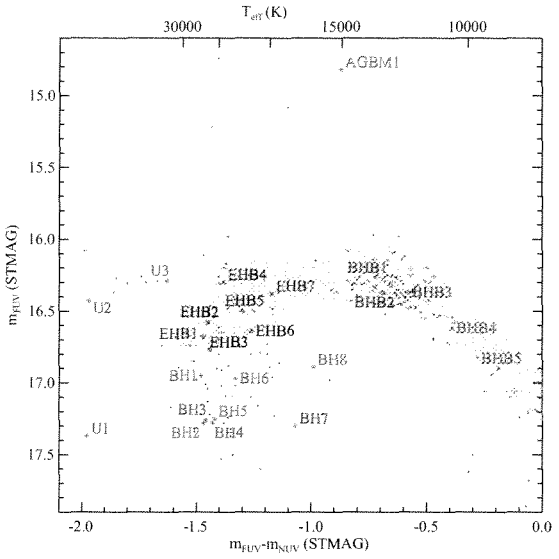

Figure 2. The UV CMD of NGC 2808 (Brown et al. 2001) with labels for those sources with clean far-UV spectroscopy (see Figure 1). The cluster was imaged with the FUV/F25QTZ and NUV/F25CN270 bandpasses on STIS (see Figure 2 of Brown et al. 2001). The photometric errors are indicated (grey crosses). The statistical uncertainty in photometric color is <0.02 mag for our entire spectroscopic sample, and the agreement between the observed and theoretical BHB locus indicates that systematic errors (e.g., instrument calibration, assumed reddening) cannot be large.

tion, and subtracts a background estimated from two neighboring extraction boxes. To reduce the noise in this background estimate, the background is smoothed before subtraction. Specifically, X1D replaces the background counts spectrum with a low-order polynomial fit to the background, except for two wavelength regions centered on the bright geocoronal lines of Lyman-α λ1215 and O I λ1301, where the background spectrum changes too rapidly to be accurately fit by a low-order polynomial. These two geocoronal lines fill the 2″ slit, such that the lines are ~50 Å wide in the gross counts spectrum, extending beyond the wavelength regions normally ignored by the polynomial fit. To accurately account for the background in the presence of these broad geocoronal lines, we turned off background smoothing in X1D, subtracted the unsmoothed background spectrum at wavelengths shorter than 1350 Å, and at longer wavelengths, subtracted a fit to the background spectrum using a Legendre polynomial.

Although the geocoronal lines are subtracted as part of the background subtraction in the X1D software, the SNR in the net spectrum is roughly an order of magnitude lower than it is outside of the regions spanned by these lines. For a star that is well-centered in the slit, the geocoronal Lyman-α line will span 1190–1240 Å in the stellar spectrum, but for a star off-center, the Lyman-α line can span a region in the wavelength-corrected stellar spectrum that is offset by ~25 Å in either direction, thus possibly including a potentially useful C III multiplet at 1175 Å. For this reason, in our analysis below, the C abundance must be derived from both this C III multiplet and C IV $\lambda\lambda$1548,1551.

After finalizing the X1D extractions, the individual spectra for each star were combined with the IRAF SPLICE package. The combined spectra are shown in Figures 3 – 10. For most of the stars, 10 such individual spectra from a single slit position were combined to produce the final spectrum, but three stars (BH2, BH5, and U3) fall in the overlap between two slit positions (see Figure 1), and thus have 20 individual spectra and twice the nominal exposure time. Comparing the spectra obtained in the two distinct slit positions for these three stars shows good agreement, providing a check on our extraction procedures. Besides the 24 hot stars with clean spectroscopy, a handful of other hot stars fell within the slit for each slit position, but we were unable to extract accurate spectra for these objects for a variety of reasons, such as overlapping spectra, spectra falling under the shadow of the detector repeller wire, spectra falling under a slit occulting bar, or spectra falling on detector artifacts.

3. MODELS

We interpret our far-UV spectra using synthetic spectra from several sources. For the unclassified object U3 and the relatively cool AGBM and BHB stars, we use the UVBLUE grid (Rodríguez-Merino et al. 2005). For the hot and nearly featureless spectra of U1 and U2, we compare to both simple blackbody models and the hottest stellar model of Rauch & Ringat (2011), which has $T_{\rm eff}$ = 250,000 K, log g =7, and mass fractions of 0.33, 0.5, 0.02, and 0.15 for He, C, N, and O, respectively. For the EHB and BH stars that are the primary focus of this paper, we calculated non-LTE line-blanketed model atmospheres and synthetic spectra, using our TLUSTY (Hubeny & Lanz 1995) and SYNSPEC programs[7].

TLUSTY computes stellar model photospheres in a plane-parallel geometry, assuming radiative and hydrostatic equilibria. Departures from LTE are explicitly allowed for a large set of chemical species and arbitrarily complex model atoms, using our hybrid Complete Linearization/Accelerated Lambda Iteration method (Hubeny & Lanz 1995). More specifically, the model atmospheres allow for departures from LTE for 1132 levels and superlevels of 52 ions: H I, He I, He II, C I – C IV, N I – N V, O I – O VI, Ne I – Ne IV, Mg II, Al II, Al III, Si II – Si IV, P IV, P V, S II – S VI, Fe II – Fe VI. Details of the model atom setup are provided in Lanz & Hubeny (2003, 2007), and in Cunha et al. (2006) for updated Ne models.

The model grid spanned 17,500 K to 47,500 K in $T_{\rm eff}$, with 2,500 K steps, and 4.75 to 6.25 in log g, with 0.75 steps. For the chemical composition, we initially began with broad abundance categories. One grid was calculated at standard cluster abundances, with [Fe/H]=–1.36, Y = 0.23, and [α/Fe]=+0.3. The other grids assumed enhanced Y values of 0.4, 0.7, and 0.99, with each value of Y accompanied by either normal C and N abundances or enhanced C and N abundances (up to 3% and 1% by mass, respectively; see Lanz et al. 2004). In order to match the absorption line equivalent widths and broader line-blanketing features in our BH and EHB spectra, we generated new models at Y = 0.23 and Y = 0.99, with the abundances of C and Si varied individually, and the abundances of the Fe-peak elements varied together but independently from the elements outside of the Fe peak. In these models, we assumed log g=5.5, which should be representative of the surface gravities in the BH and EHB stars, given the insignificant variations in the low-resolution far-UV spectral features over the full range of surface gravity in such stars.

After the detailed emergent UV spectrum for each model atmosphere was calculated with SYNSPEC, they were shifted to the radial velocity of NGC 2808 (101.6 km s^{-1}; Harris 1996). We then added the absorption from strong interstellar lines of H I (1.9×10^{21} cm^{-2}), C II (6.8×10^{18} cm^{-2}), C IV (6.0×10^{17}

[7] Available at http://nova.astro.umd.edu

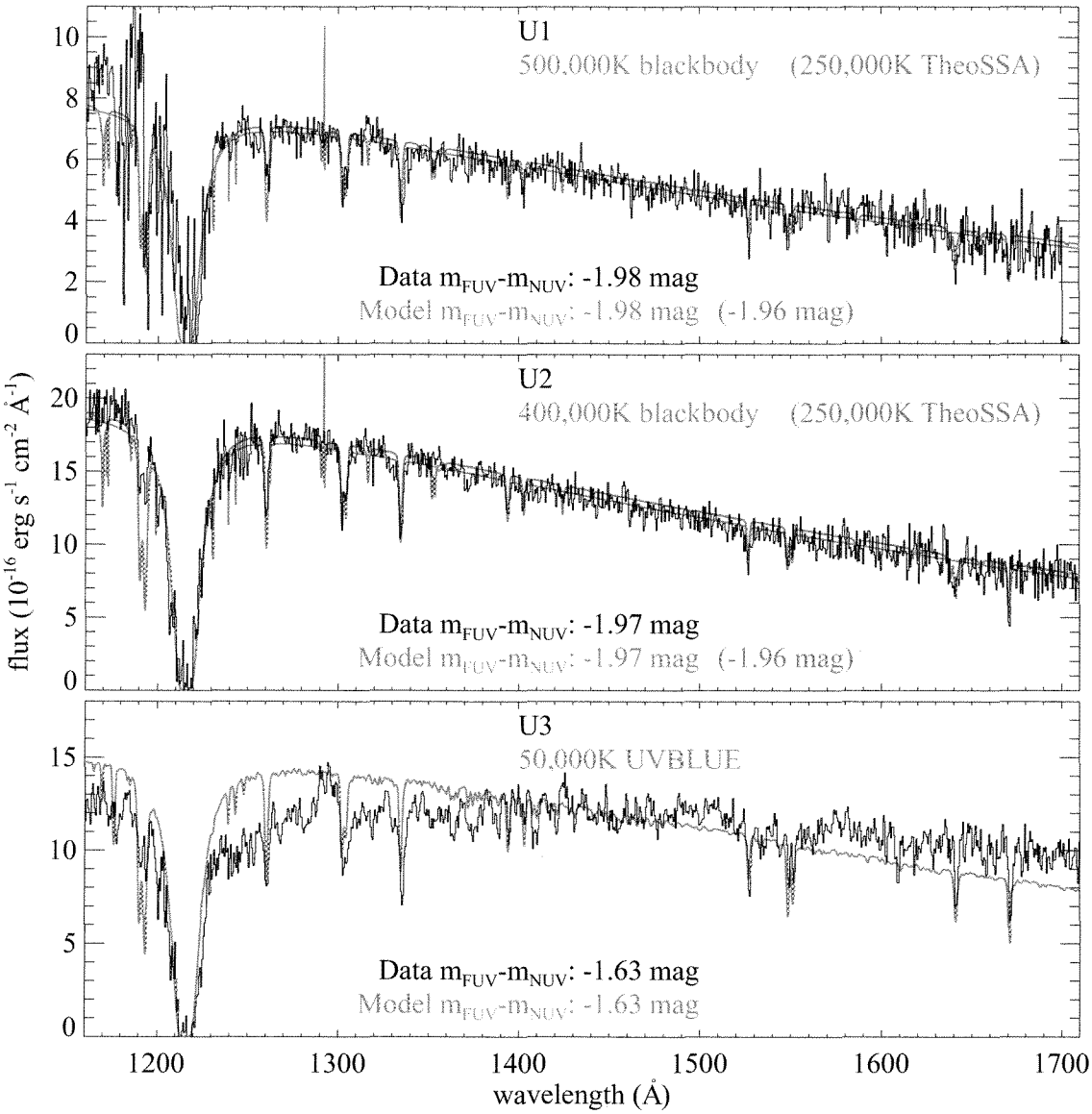

Figure 3. The spectra of our 3 unclassified objects (black histograms). In the top two panels, we compare the U1 and U2 spectra to blackbody models (green curves and labels) that approximately reproduce the far-UV spectral slope and the $m_{FUV}-m_{NUV}$ color, although the assumed temperatures are unphysically hot. We also compare these spectra to the hottest synthetic spectrum in the TheoSSA database (purple curves and labels; Rauch & Ringat 2011). U1 and U2 are nearly featureless, other than interstellar absorption features and the He II absorption at 1640 Å. In the bottom panel, the UV photometry of U3 is consistent with a 50,000 K photosphere, but its UV spectrum looks much flatter than one would expect for this temperature. For comparison, we show the synthetic spectrum of a 50,000 K star at [Fe/H] =−1.36 (green curve), interpolated from the UVBLUE grid (Rodríguez-Merino et al. 2005).

cm^{-2}), Si II (1.7×10^{17} cm^{-2}), Si IV (7.6×10^{16} cm^{-2}), O I (6.0×10^{18} cm^{-2}), and Al II (5.0×10^{16} cm^{-2}), using the observed spectra of U1 and U2 as a guide (Figure 3), given the lack of obvious photospheric features in these spectra (aside from He II). Our assumed H I column is nearly twice what one would expect from the mean gas-to-dust ratio in the Galaxy (e.g., Bohlin et al. 1978), but there are significant variations in this ratio along any given sightline (e.g., Diplas & Savage 1994). It is also larger than the column of 1.2×10^{21} cm^{-2} found in the x-ray analysis of Servillat et al. (2008), but a column that low is strongly discrepant with the Lyman-α profile in our spectra. We then reddened the spectrum using the mean Galactic extinction curve of Fitzpatrick (1999), assuming $E(B-V) = 0.18$ mag (Brown et al. 2001, 2010).

4. ANALYSIS

4.1. *Comparison of the Combined EHB and BH Spectra*

We begin our analysis with an empirical look at the spectra of the EHB and BH samples. The stars in each sample span a similar range of $m_{FUV}-m_{NUV}$ color, but the BH stars are ~0.7 mag fainter than the EHB stars (Figure 2). In Figure 11, we show the average spectrum for all 7 of the normal EHB stars in our sample, compared to the average spectrum for all 8 of the BH stars (i.e., subluminous EHB stars) in our

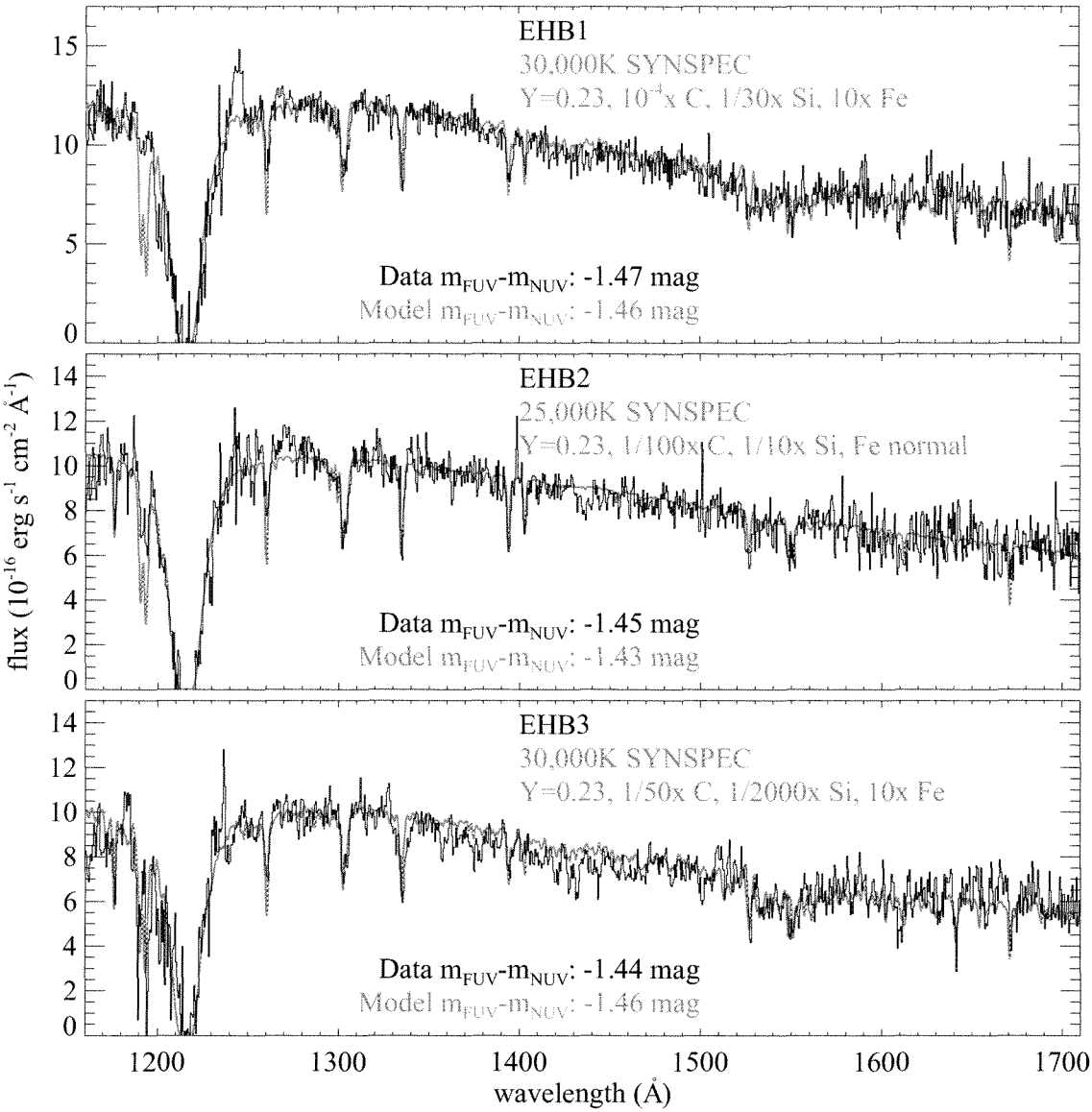

Figure 4. The spectra of three normal EHB stars (black histograms) compared to SYNSPEC synthetic spectra (green curves) that approximately match the UV photometry and spectroscopy. The stars exhibit large abundance variations relative to the mean cluster abundance at the MS (labeled), presumably due to atmospheric diffusion. Data points with potential instrumental artifacts are flagged (red diamonds).

sample. Several strong features are due almost exclusively to interstellar absorption, and are similar in both of the composite spectra: Si II λ1260 Å, O I λ1301 Å, Si II λ1304 Å, C II λ1335 Å, Si II λ1527 Å, and Al II λ1670 Å. At these temperatures, the Si IV $\lambda\lambda$1394,1403 doublet has significant contributions from both photospheric and interstellar absorption, but the strength of this feature is similar in both composite spectra, implying that on average, there is not much difference in Si abundance between the two populations. The Lyman-α feature in these spectra is dominated by interstellar absorption, but the BH composite spectrum clearly exhibits less Lyman-α absorption. Given the dominant contribution from interstellar absorption in this feature, the photospheric absorption must be much weaker in the BH stars than in the EHB stars, in order to produce a noticeable difference in the combined interstellar and photospheric feature. The presence of weaker Lyman-α absorption in the BH stars is consistent with both higher temperatures and/or a higher He abundance in the atmospheres of the BH stars, which is what one would expect if the BH stars are flash-mixed. Besides this difference in Lyman-α, there are strong distinctions between the BH and EHB stars in three other absorption features: C III λ1176 Å(a multiplet of 6 lines), C IV $\lambda\lambda$1548,1551 Å, and He II λ1640 (a triplet). The C III and He II features are purely photospheric, while the C IV feature includes both interstellar and photospheric contributions. The C and He features are clearly stronger in the composite BH spectrum, as expected if the BH stars are flash-mixed. These features become stronger at the higher abundances and higher temperatures expected in

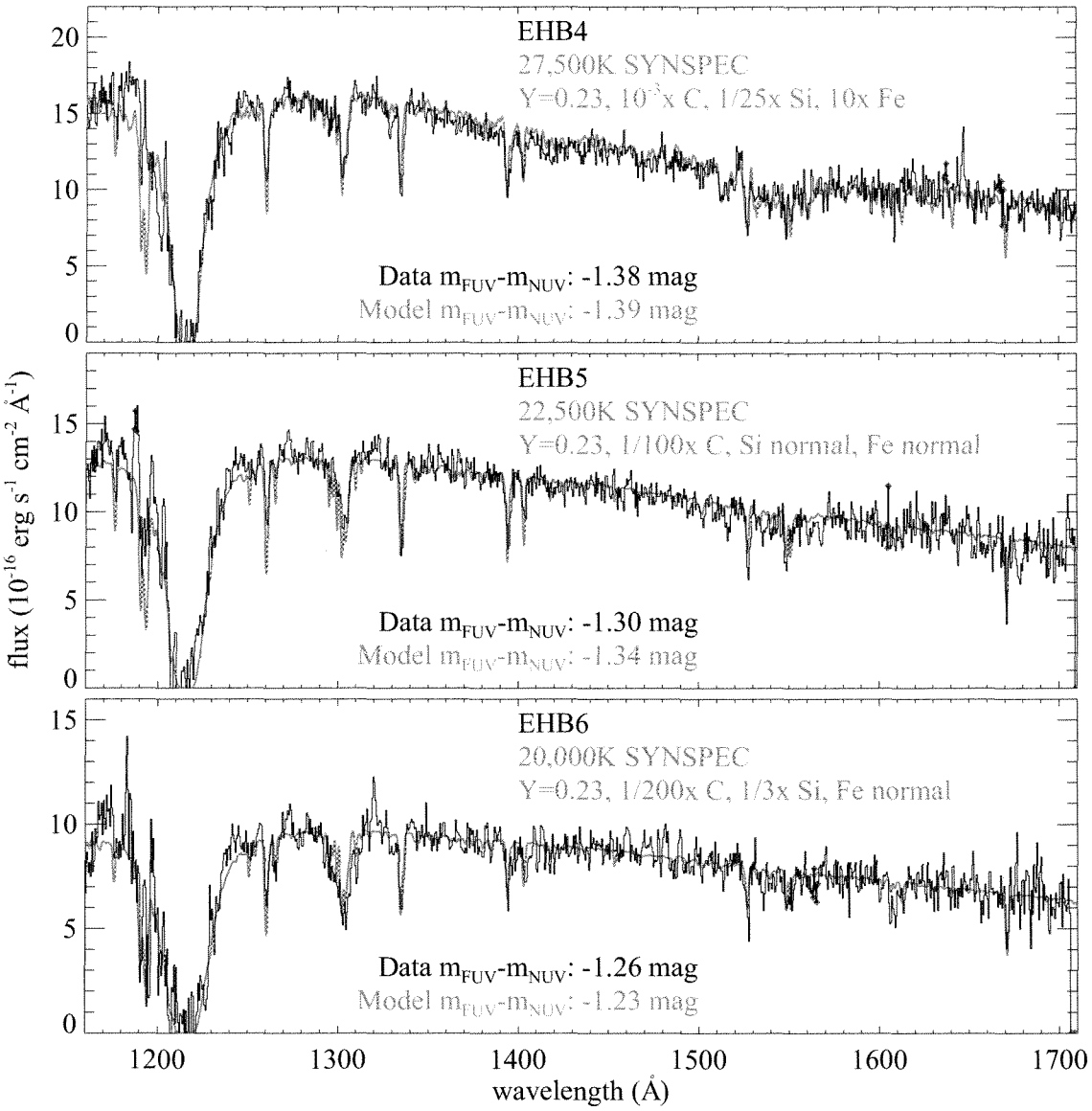

Figure 5. As in Figure 4, but for another three EHB stars with normal luminosities (black histograms) compared to SYNSPEC synthetic spectra (green curves).

flash-mixed stars (Brown et al. 2001).

4.2. *Individual EHB and BH Spectra*

We next turn to the individual spectra of the EHB and BH stars in our sample. As stated earlier, our synthetic spectra were computed on a $T_{\rm eff}$ grid with 2,500 K spacing, initially employing broad abundances classes. For each star, we first selected a synthetic spectrum that reproduced the gross characteristics of the observed spectrum and photometry, and then altered the abundances of C, Si, and the Fe-peak elements to match the observed atmospheric features. At the resolution and SNR of our spectra, estimating the equivalent width is hampered by the determination of the reference pseudo-continuum level in the presence of so many other lines. However, the data are of sufficient quality to characterize gross distinctions in abundance, at the level needed to detect the signature of flash mixing. We will specify the abundances of these three elements as multipliers on the abundances one would expect from a population at [Fe/H] = −1.36 with [α/Fe] = 0.3, to make it more straightforward to interpret these abundances as changes incurred during the evolution from the MS. However, it is worth repeating that NGC 2808 hosts a triple main sequence (D'Antona et al. 2005; Piotto et al. 2007), with the reddest and bluest sequences exhibiting clear chemical distinctions (Bragaglia et al. 2010), in particular a 0.4 dex C depletion in the bluest MS stars, relative to the reddest MS stars.

Although the composite spectra of the BH and EHB samples in Figure 11 show no obvious systematic difference in the Si abundance between the two classes, the Si abundance does show large star-to-star variations within each group (Figures 3–8). Most of the detectable Si features in our far-UV spectra are dominated by interstellar absorption, and none are com-

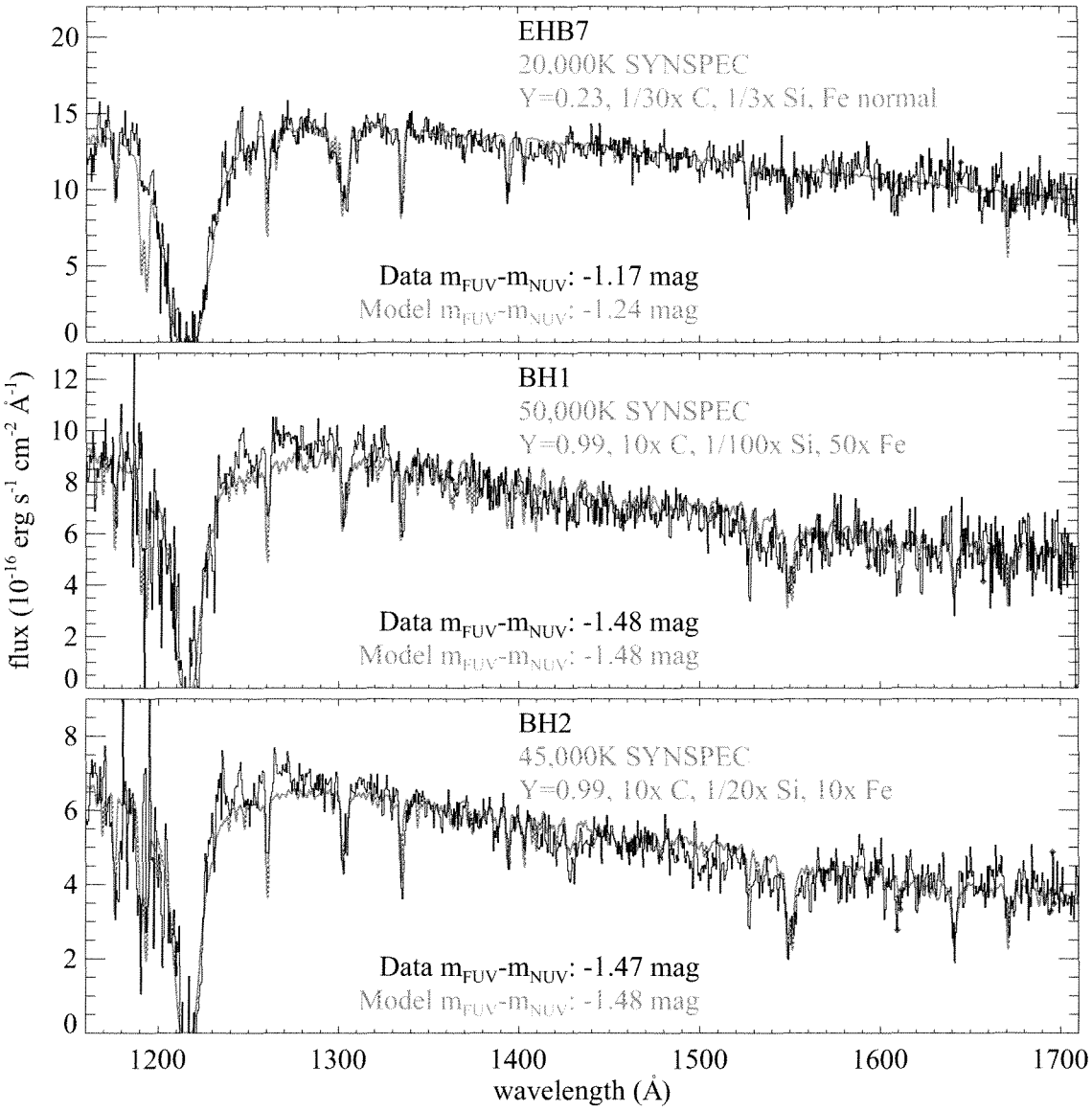

Figure 6. As in Figure 4, but for a normal EHB star and two BH stars (black histograms) compared to SYNSPEC synthetic spectra (green curves). The BH stars exhibit much stronger He and C lines than the normal EHB stars.

pletely photospheric, but Si IV $\lambda\lambda$1394,1403 Å does provide an indication of the stellar Si abundance. One star (EHB5; Figure 5) exhibits a Si abundance close to the cluster value, but most of the EHB and BH stars exhibit weak to strong depletion of Si relative to the cluster value. In BH5, BH6, and BH7 (Figures 7 & 8), Si is depleted by at least a factor of 1000, although at these low photospheric abundances, the Si IV feature is almost completely dominated by interstellar absorption, and the photospheric abundance we measure is an approximate upper limit.

With these spectra, there are no sufficiently isolated absorption lines from the Fe-peak elements that can be used to accurately characterize their abundances. However, the Fe-peak elements do cause broad absorption troughs in the far-UV spectrum that require large changes in the Fe-peak abundances in order to match the observed variations in the pseudo-continuum. The most obvious examples of this absorption can be seen in BH7 and BH8 (Figure 8), where the Fe-peak abundances are enhanced over the cluster value by factors of 25 and 100, respectively. Brown et al. (2001, 2010) have noted that some of the BH stars in massive globular clusters are curiously red – much redder than one would expect from models for either normal EHB stars or BH stars. BH7 and BH8 are in this group of curiously red BH stars. Our spectra for these BH stars show that their red colors can be explained by a large enhancement in their abundances of the Fe-peak elements. For comparison, models at the mean cluster abundance can match the $m_{FUV} - m_{NUV}$ colors of BH7 and BH8 only at much cooler temperatures of 16,900 K and 15,600 K, respectively; however, at such temperatures, the

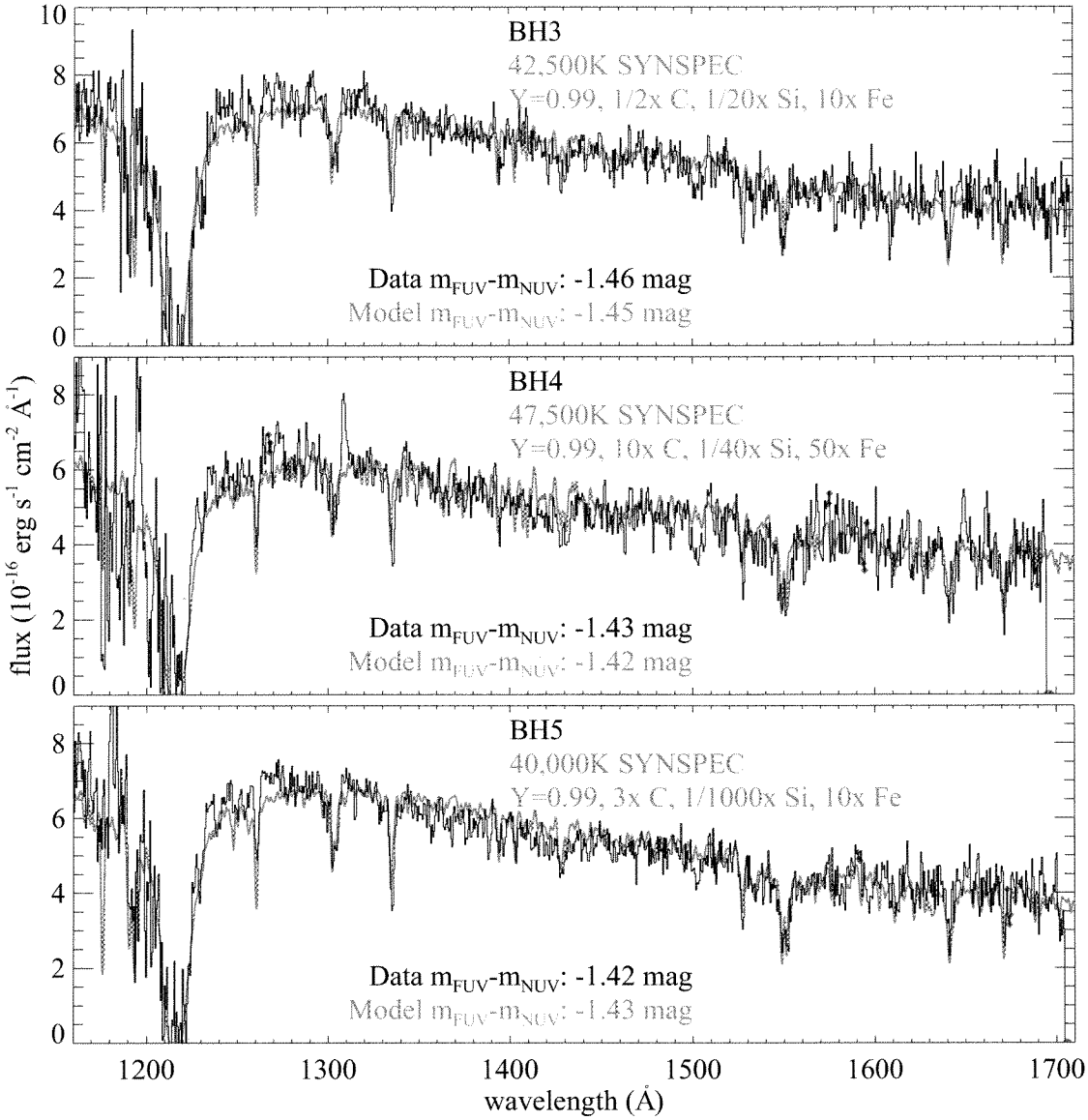

Figure 7. As in Figure 4, but for three more BH stars (black histograms) compared to SYNSPEC synthetic spectra (green histograms).

shape of the far-UV continuum in the synthetic spectra looks nothing like that observed. These large Fe-peak enhancements are required for the model to reproduce both the UV photometry and spectroscopy simultaneously. All of the BH stars show Fe-peak enhancements, ranging from 10× to 100× the cluster value, while the EHB stars are mixed, with three showing a 10× enhancement and the other four showing no evidence for enhancement.

There are three significant C features in the far-UV spectra: the purely photospheric feature at 1176 Å from the C III multiplet, the purely interstellar feature at 1335 Å from the C II multiplet, and the C IV λλ1548,1551 doublet that has both photospheric and interstellar contributions. Although the C III feature provides the potentially cleanest indicator of the stellar C abundance, in practice it frequently suffers from low SNR, relative to the C IV feature. This is because the C III feature is affected to a varying degree by the Lyman-α geocoronal line (see §2). For this reason, we try to match the strength of both the C III and C IV features. In all of the EHB stars, the C abundance is depressed relative to that in the cluster, to varying degrees: C is depressed by a factor of 30 in EHB7, whereas C is nearly undetectable in EHB1, where it is depressed by a factor of 10,000. In the BH sample, five of the stars (BH1, BH2, BH4, BH5, and BH7) are enhanced in C (by factors of 3 to 10), two of the stars (BH3 and BH8) are somewhat depressed in C (by factors of 2 to 10), and one star (BH6) is significantly depressed in C (by a factor of 400).

There is one significant He feature in the far-UV spectra: the purely photospheric He II feature at 1640 Å. At the temperatures of EHB and BH stars, the feature is mildly sensitive to abundance and very sensitive to $T_{\rm eff}$. Furthermore, for

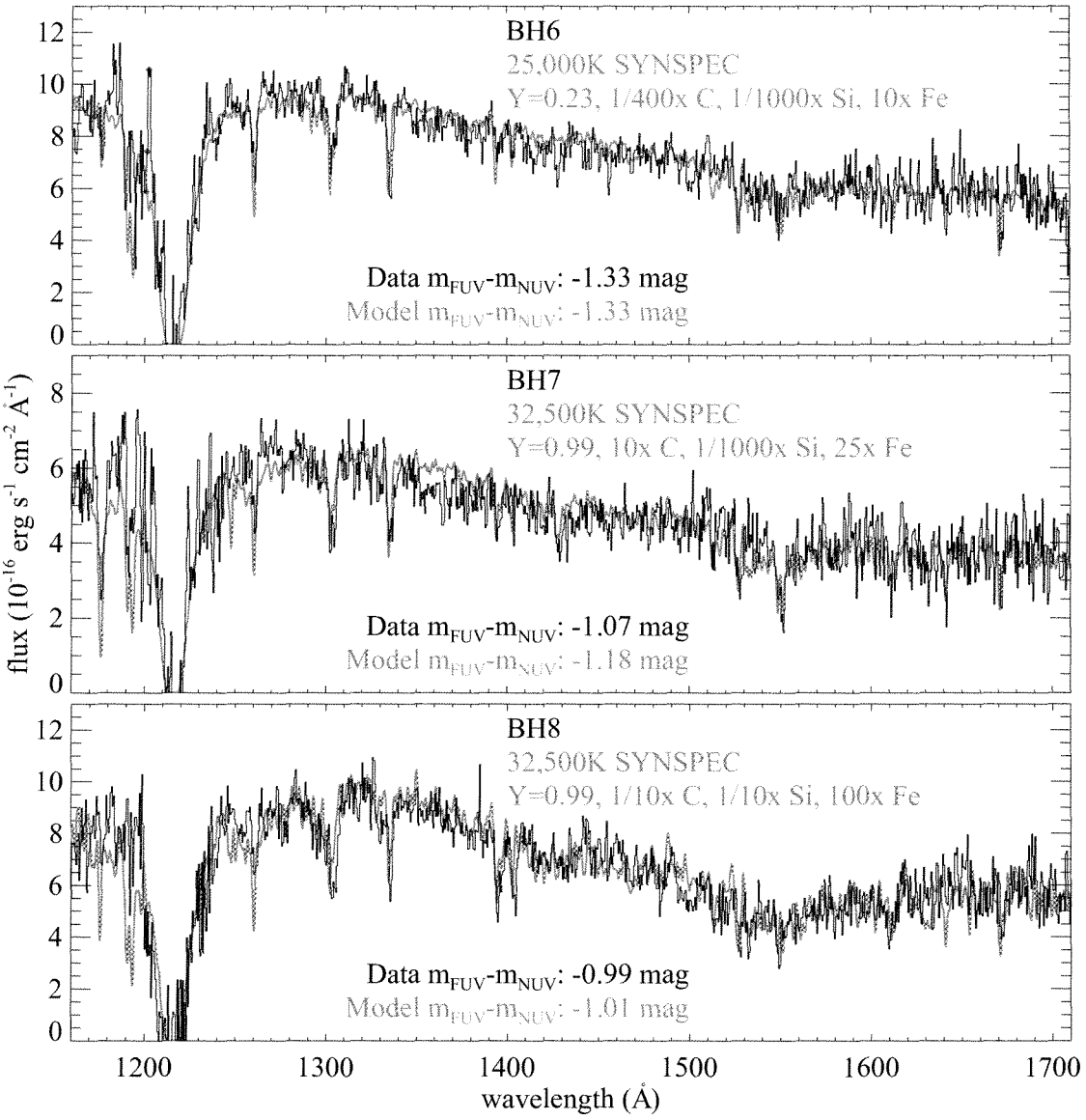

Figure 8. As in Figure 4, but for three more BH stars (black histograms) compared to SYNSPEC synthetic spectra (green histograms). Unlike the other BH stars in our spectroscopic sample, BH6 shows no He and C enhancement, is relatively cool, and has a luminosity not much below the luminosity of the canonical EHB, so it is likely that the star did not undergo flash mixing. Compared to most of the BH stars in our photometric sample, BH7 and BH8 have unusually red UV photometry, which may be explained by the strong enhancement of Fe, presumably due to atmospheric diffusion. Although the BH8 spectrum does not exhibit a strong He II feature at 1640 Å, an enhanced He abundance in the model is needed to match both the UV photometry and far-UV spectroscopic continuum simultaneously (see text).

these temperatures, the $m_{FUV} - m_{NUV}$ color does not significantly change if the He abundance is increased from $Y = 0.23$ to $Y = 0.4$, but it becomes ~0.1–0.3 mag redder if the He is increased to $Y = 0.99$. For this reason, the He abundance must be constrained by matching the far-UV spectral slope, the $m_{FUV} - m_{NUV}$ color, and the He II absorption feature simultaneously. In the EHB sample, these three aspects of each star can be matched by a model at the standard cluster He abundance ($Y = 0.23$). The He II feature is only obvious in the spectra of EHB1 and EHB3, which are the hottest stars in our EHB sample, at 30,000 K. In the BH sample, the He II feature is extremely strong in six of the stars (BH1, BH2, BH3, BH4, BH5, and BH7), even though these stars have $m_{FUV} - m_{NUV}$ colors that are similar to those in the EHB sample. To simultaneously match the $m_{FUV} - m_{NUV}$ color and He II feature in each of these stars, the synthetic spectra must be much hotter than those used to match the EHB sample, with an atmosphere that is 99% He by mass.

To see why this is the case, we can compare stars in the EHB and BH samples that have similar $m_{FUV} - m_{NUV}$ colors. For example, EHB1 (Figure 4) and BH2 (Figure 6) have exactly the same $m_{FUV} - m_{NUV}$ color (−1.47 mag), they both exhibit enhanced abundances of the Fe peak elements (10 times larger than the cluster mean), and they have sim-

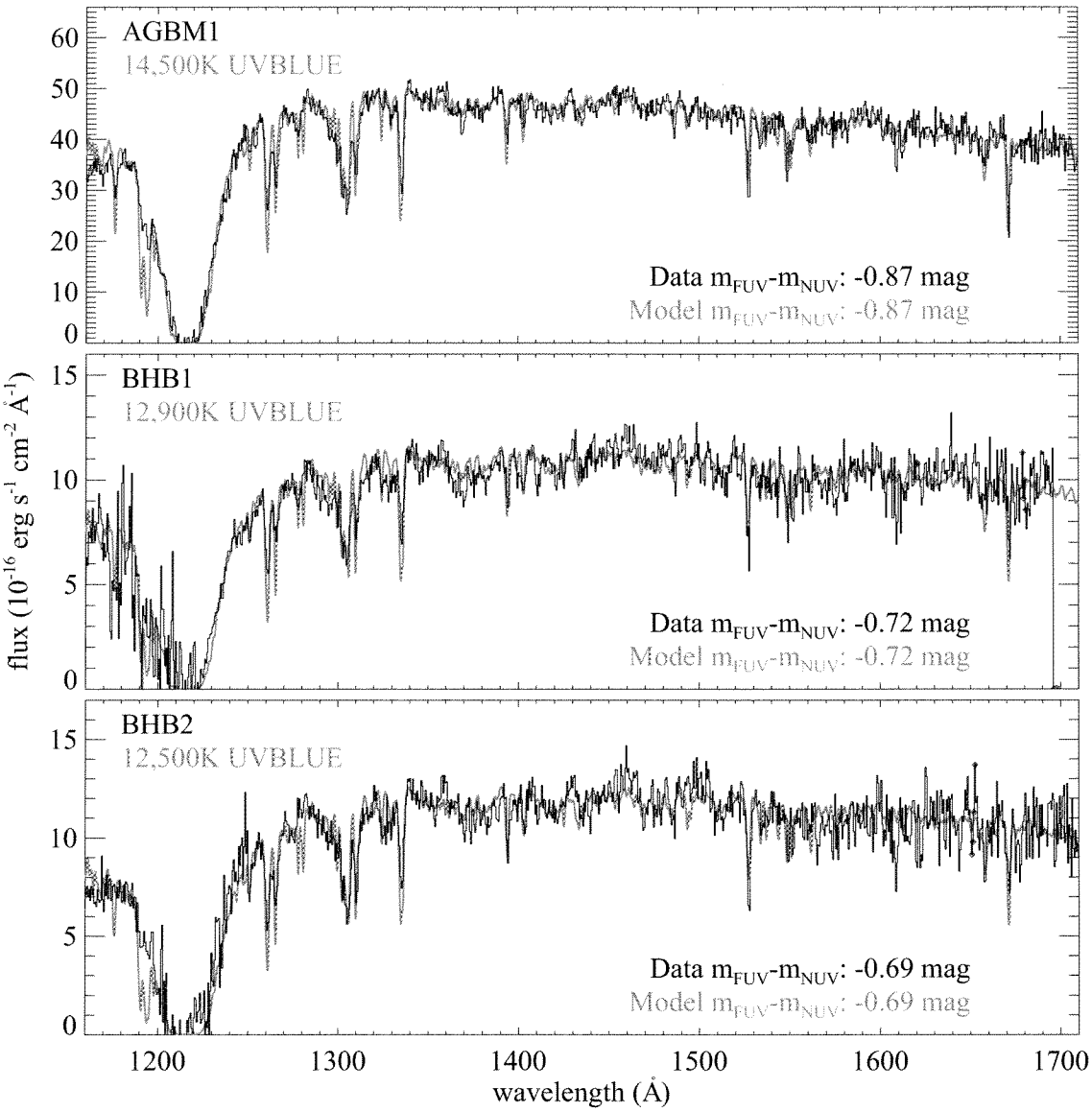

Figure 9. As in Figure 4, but for an AGBM star and two normal BHB stars (black histograms) compared to UVBLUE synthetic spectra (green curves). The synthetic spectra were interpolated in temperature and metallicity from the UVBLUE grid to match the $m_{FUV} - m_{NUV}$ color at the cluster metallicity.

ilar Si abundances (20 to 30 times lower than the cluster mean). However, the BH2 spectrum has much stronger C IV and He II lines than the spectrum of EHB1. The EHB1 spectrum is well-matched by a model at 30,000 K, but the BH2 spectrum requires a model that is 15,000 K hotter. If one takes the BH2 model shown in Figure 6 and reduces Y from 0.99 to 0.23 (while holding all other parameters fixed), the $m_{FUV} - m_{NUV}$ color increases to −1.6 mag, which is far bluer than the -1.43 ± 0.014 mag observed. Only a He-rich model reproduces the spectral slope, He II feature, and $m_{FUV} - m_{NUV}$ color. A similar argument can be made comparing EHB4 (Figure 5; $T_{\rm eff}$=27,000 K, $m_{FUV} - m_{NUV}$=−1.38, 10× enhanced Fe-peak elements, 25× depleted Si) and BH5 (Figure 7; $T_{\rm eff}$=40,000 K, $m_{FUV} - m_{NUV}$=−1.42, 10× enhanced Fe-peak elements, 1000× depleted Si); EHB4 has very weak C IV absorption and no detectable He II absorption, while BH5 has extremely strong C IV and He II absorption.

While most of the BH sample exhibits obvious He enhancement, there are exceptions. The photometry and spectroscopy of BH6 can be matched by a model that has a relatively low $T_{\rm eff}$ (25,000 K), depleted C abundance (400× lower than the cluster value), and $Y = 0.23$. The BH8 spectrum does not appear to have a strong He II feature, but a $Y = 0.99$ model is required to simultaneously match the photometry and spectroscopic slope; reducing Y to 0.23, while holding the other parameters fixed, does not significantly impact the agreement with the far-UV spectrum, but makes the model $m_{FUV} - m_{NUV}$ color 0.3 mag bluer. Similar to BH6, the BH8 spectrum indicates a C abundance depleted with respect to the cluster value, although it is still much higher than that in the EHB sample.

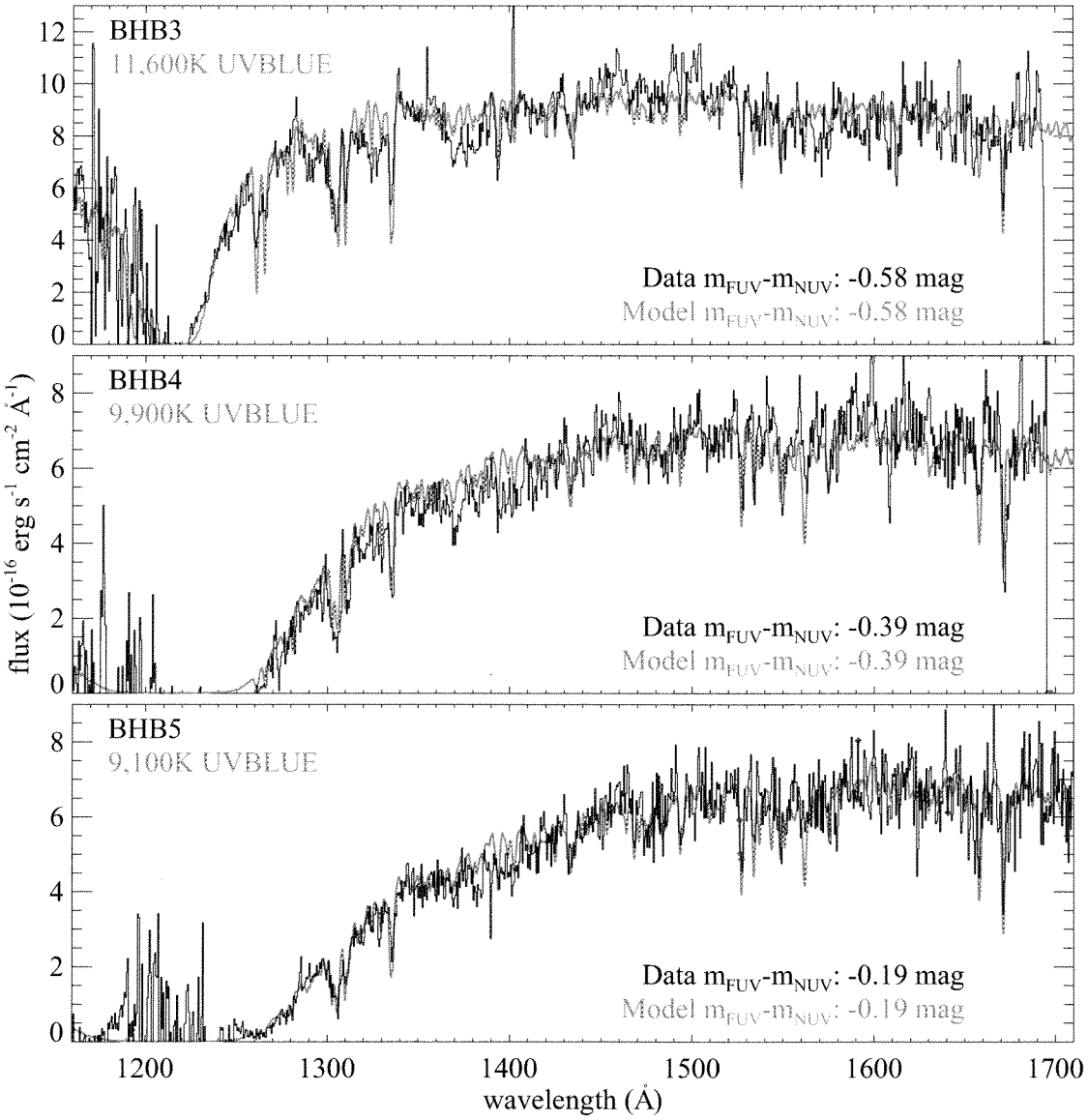

Figure 10. As in Figure 4, but for three more normal BHB stars (black histograms) compared to UVBLUE synthetic spectra (green curves).

To summarize, the EHB stars and BH stars exhibit no systematic difference in Si abundance, but both classes exhibit large star-to-star variations in Si abundance, probably resulting from atmospheric diffusion. The Fe abundance also varies strongly from star to star, but it is systematically higher in the BH stars than in the EHB stars, and all of the BH stars exhibit large Fe enhancements. The largest chemical distinctions between the EHB and BH stars are those related to flash mixing (He and C). All of the EHB stars exhibit C abundances much lower than the cluster value, and He abundances at or below the solar value. As a group, the BH stars are significantly hotter than the EHB stars, with five of them exhibiting enhanced C, and seven of them exhibiting enhanced He, which is strong evidence that most of the BH population arises from flash mixing. The fact that He and C are not enhanced in the full BH sample may indicate that some of these stars did not undergo flash mixing (e.g., BH6), or that these elements were depleted due to atmospheric diffusion (e.g., BH3 and BH8; see Miller Bertolami et al. 2008).

4.3. *Hot Unclassified Stars*

Although the focus of this project is a comparison of the EHB and BH samples in NGC 2808, our spectroscopic sample includes 9 other hot stars, which we briefly discuss here. Three of these stars (U1, U2, and U3) are hotter than the canonical HB (see Figure 2), and are labeled as unclassified. As with our BH and normal EHB samples, the photometric uncertainties on these stars are small (see Figure 2), and there does not appear to be anything unusual about them in the UV images of the cluster (e.g., they do not appear to be blends, or to suffer from a detector artifact). Both U1 and U2 are hotter (bluer) than the evolutionary path a low-mass

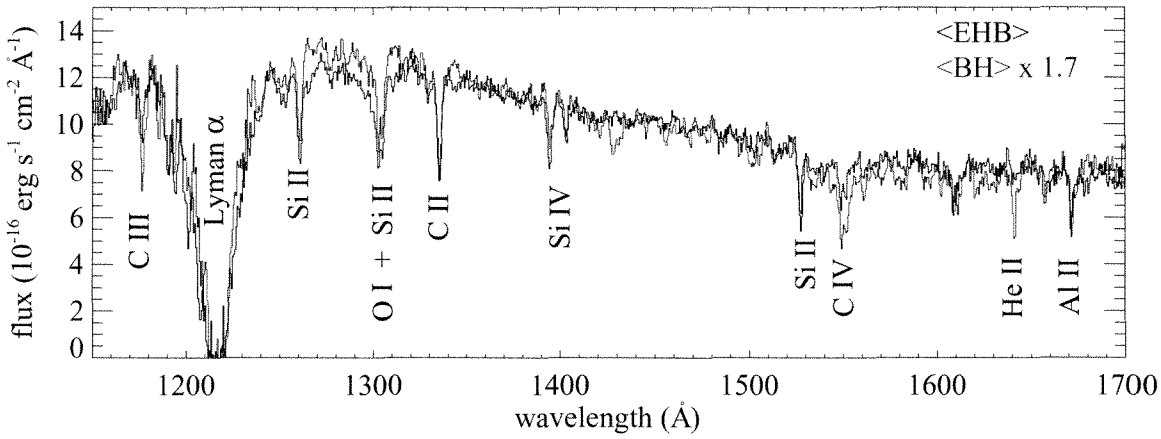

Figure 11. The composite spectrum for all EHB stars (black histogram) compared to that for all BH stars (blue histogram), with the latter normalized by 1.7.

star would take through the HR diagram as it begins to descend the white dwarf cooling curve, and they are also significantly brighter than the part of the white dwarf cooling curve where stars would begin to appear in any significant numbers, given the speed of the evolution between the HB and the white dwarf phases (e.g., see Figure 3 of Brown et al. 2001). The $m_{FUV} - m_{NUV}$ colors of U1 and U2 are implausibly blue compared to the expectations from evolutionary tracks for single stars, and the spectroscopy of these objects confirms that they are extremely hot (see Figure 3). U1 and U2 are consistent with blackbody temperatures of 400,000 K and 500,000 K, respectively, although both the UV photometric color and far-UV spectroscopic slope are becoming degenerate with temperature at such temperatures. More physically plausible would be the synthetic spectrum of a hot star. The hottest model in the TheoSSA database of synthetic spectra for hot compact stars has a temperature of 250,000 K, and is in reasonable agreement with the UV spectral slope and photometry (Figure 3). However, if U1 and U2 have effective temperatures near 250,000 K, neither is actually compact; stars at that temperature and the far-UV luminosities we observe would have radii similar to that of a low-mass post-AGB star that is about to descend the white dwarf cooling curve. The luminosities of U1 and U2 would be $\log L/L_{\odot}$ =3.1 and 3.5, respectively; such a high luminosity is at the extreme limit of that found for any globular cluster post-AGB star, and such temperatures are a factor of two higher than those found in low-mass post-AGB tracks. Note that some estimates for the foreground extinction toward NGC 2808 are higher than our value of $E(B-V) = 0.18$ mag. For example, Harris (1996) obtains $E(B-V) = 0.22$ mag from his assessment of the literature. Assuming a higher extinction would imply that even hotter intrinsic temperatures for U1 and U2 are needed to match the observed photometry and spectroscopy, but another possibility is that the extinction along the NGC 2808 sightline differs from the Galactic mean curve. Neither U1 or U2 appear to be coincident with x-ray sources in NGC 2808 (Servillat et al. 2008), but perhaps these objects are associated with accretion disks that could explain their unusually hot temperatures.

The unclassified star U3 is very puzzling. It has a very blue $m_{FUV} - m_{NUV}$ color in the NGC 2808 photometry, but its far-UV spectrum is much flatter than one would expect from a star with these UV colors. Perhaps the photometry and spectrum are the result of some kind of blend, non-stellar source, and/or circumstellar extinction, but we are unable to put forth a plausible explanation for the object. Like U1 and U2, U3 is not coincident with x-ray sources in NGC 2808 (Servillat et al. 2008). U2 and U3 respectively define the blue and red ends of a curious string of stars bluer than the canonical HB but all sharing approximately the same luminosity (see Figure 2).

4.4. *BHB and AGBM Spectra*

The AGBM and BHB stars in Figures 9 and 10 are well-matched by spectra from the UVBLUE (Rodríguez-Merino et al. 2005) grid, once these are interpolated to the NGC 2808 mean metallicity of [Fe/H]=−1.36 and to the effective temperatures that match the $m_{FUV} - m_{NUV}$ colors. The UVBLUE spectra do not provide the ability to independently vary individual elements, but the comparison between the synthetic spectra and data shows no gross signatures of atmospheric diffusion. The equivalent widths of the C and Si lines in our observed spectra are approximately matched by the lines in the synthetic spectra, although the C and Si lines are mostly dominated by interstellar absorption at these cooler temperatures. Furthermore, our AGBM and BHB spectra do not exhibit broad absorption troughs from the Fe-peak elements, indicating that the abundances of the these elements are not greatly enhanced. This was unexpected, because our BHB sample brackets the temperature (∼11,500 K) where the radiative levitation of metals causes a discontinuity in Stromgröm photometry of several globular clusters (Grundahl et al. 1999). In the globular cluster M13, which has a metallicity of [Fe/H] =−1.5 (i.e., only slightly lower than that of NGC 2808), the BHB stars hotter than this temperature exhibit an enhancement in the Fe abundance that approaches three times the solar abundance (Behr et al. 1999) – one to two orders of magnitude higher than cooler BHB stars and the mean cluster abundance. In NGC 2808 itself, Pace et al. (2006) found that BHB stars at or below 12,000 K exhibited no Fe enhancement, but that the Fe abundance increases to ∼–0.7 at 12,200 K, ∼0.1 at temperatures of 12,400–12,800 K, and then ∼0.5–1.0 for stars hotter than 13,000 K. Assuming the same relationship between Fe enhancement and $T_{\rm eff}$ applies in our own sample, we would expect no enhancement in BHB3, BHB4, and BHB5, but enhancements of one to two orders of magnitude in BH1 and BH2. Such enhancements would be very obvious in the BH1 and BH2 spectra, but it is clear from Figures 9 and 10 that

there is, in fact, little distinction in Fe abundance between BHB2 and BHB3 (the two stars bracketing the temperature of this transition). This does not seem to be due to any obvious systematic errors in our assumptions. For example, one can reproduce the $m_{FUV}-m_{NUV}$ color of BHB1 by assuming a significantly lower extinction of $E(B-V)=0.13$ mag in conjunction with a temperature of 12,000 K, which would place BHB1 at a temperature where it would not be expected to exhibit an Fe enhancement. However, the resulting far-UV synthetic spectrum has a Lyman-α profile much wider than that observed, and the extinction would be much lower than most values adopted in the literature, including that of Pace et al. (2006), who assumed $E(B-V)=0.22$ mag in their analysis.

The star AGBM1 is far brighter than the other stars in our sample, and its spectrum has the highest SNR. Although the observed spectrum is generally well-matched by the interpolated UVBLUE spectrum, there is a discrepancy in the strength of the interstellar Si II feature at 1190 Å (which arises from our interstellar absorption model, and not the UVBLUE grid). Although this feature falls within the region where the SNR is depressed by the broad geocoronal Lyman-α line, the luminosity of this particular star means it still has adequate SNR to accurately measure this feature if present. In fact, the Si II λ1190 Å feature is overpredicted by our interstellar absorption model for all of the stars in our entire sample, but our chosen Si II column does reproduce the other interstellar Si II features in the spectra.

5. DISCUSSION

Compared to the stars in our EHB sample, the stars in our BH sample are significantly hotter, and have much higher He and C abundances. This can be seen from both an empirical comparison of the mean spectrum for each class, and also from a comparison of the models that best reproduce the individual stars in each class. NGC 2808 likely hosts a sub-population of MS stars born with an enhanced He abundance ($Y\sim0.4$; D'Antona et al. 2005; Piotto et al. 2007), and such stars are more likely to produce EHB stars (including the EHB stars of normal luminosity and the subluminous BH stars). However, the flash-mixing scenario is the only plausible mechanism for producing the higher temperatures and enhanced He and C abundances in our in our BH sample.

Although the C abundance in our BH sample is greatly enhanced relative to the EHB sample, it is not as high as one would expect for stars that underwent flash mixing very recently. The strongest enhancements of C in our BH sample are at 10× the cluster ratio of C to H, corresponding to a mass fraction of 0.2% in the atmosphere, whereas flash mixing is expected to produce stars with atmospheric C abundances of 1–4% by mass. The reduction in C abundance is not unexpected, however. Miller Bertolami et al. (2008) calculated numerical simulations of stars as they evolved through the flash-mixing stage and subsequent period of stable core He burning, taking into account the atmospheric diffusion processes of gravitational settling and radiative levitation. They found that stars emerge from the flash-mixing process with strongly enhanced He and C abundances, but that the C abundance declines rapidly, dropping by an order of magnitude after 1000 yr, and by several orders of magnitude by the time the star has evolved for some 10^7 yr after the flash mixing of the envelope. Thus, the star spends only a very small fraction of its stable core He-burning lifetime wit a C abundance near its maximum of 1–4% by mass. Their calculations also show the He will eventually decline in the atmosphere as well, although this happens over a much longer timescale, such that the decline does not become significant until $\sim10^6$–10^7 yr later. The fact that Lanz et al. (2004) found higher C abundances in two of the three He-sdB stars in their Galactic field sample may be a selection effect; in NGC 2808, the stars were selected by position in the UV CMD, but the Galactic field, the stars were by He abundance.

The variations in Si and Fe-peak abundances clearly demonstrate that atmospheric diffusion is significant in the EHB and BH populations. Abundance anomalies have also been well-documented in the field population of sdB stars (e.g., see Heber 2009 and references therein), where large enhancements in the Fe-peak elements (but not Fe itself) are observed. However, recent calculations demonstrate that other processes, such as turbulent mixing and mass loss, also play a role in these anomalies (Hu et al. 2011). Our observations demonstrate that large enhancements in the Fe-peak elements can play a role in the BH phenomenon, and may explain those BH stars with unusually red UV colors (Brown et al. 2001, 2010). Two of the BH stars in our spectroscopic sample were drawn from this unusually red segment of the BH population in NGC 2808, and both exhibit enormous enhancements in the Fe-peak elements (25–100× the cluster value). Apparently a large dispersion in the abundances of Fe-peak elements, when combined with flash mixing, can provide the large color range observed in the BH population of massive clusters.

The hottest BH stars in our sample fall at temperatures similar to those of recently-discovered pulsating subdwarfs in ω Cen (Randall et al. 2011). The four pulsating subdwarfs in ω Cen are located near the BH region of the ω Cen CMD, and Randall et al. (2011) derive 48,000 K $\lesssim T_{\rm eff} \lesssim$ 52,000 K from their optical spectroscopy. Randall et al. (2011) suggest that their pulsators may be sdO stars inhabiting a newly-discovered instability strip; if that is the case, our hottest BH stars (BH1 & BH4) may also be pulsators. The enhanced Fe-peak abundances observed in our hottest BH stars may be significant, as radiative levitation appears to play a role in sdO pulsations (Fontaine et al. 2008). We note, however, that Randall et al. (2011) found subsolar He abundances for their pulsators, in contrast to the He-rich atmospheres found in our hottest BH stars. One intriguing possibility is that the pulsators in ω Cen are evolved from BH stars, which are known to exist in ω Cen; diffusion processes can convert a He-rich BH stars into a He-poor sdO (Miller Bertolami et al. 2008). If flash mixing is required to achieve these high EHB temperatures, then the dearth of analogous pulsators in the field population may be explained; flash mixing is more likely to occur in populations born at high He abundance ($Y\sim0.4$), such as those subpopulations found in massive globular clusters.

Support for Program 11665 was provided by NASA through a grant from STScI, which is operated by AURA, Inc., under NASA contract NAS 5-26555. The TheoSSA service (http://dc.g-vo.org/theossa) used to retrieve a theoretical spectrum for this paper was constructed as part of the activities of the German Astrophysical Virtual Observatory.

REFERENCES

Anderson, J. 1997, Ph.D. thesis, UCB

Behr, B.B., Cohen, J.G., McCarthy, J.K., & Djorgovski, S.G. 1999, ApJ, 517, L135

Bohlin, R.C., Savage, B.D., & Drake, J.F. 1978, ApJ, 224, 132
Bragaglia, A., et al. 2010, ApJ, 720, L41
Brown, T.M., Sweigart, A.V., Lanz, T., Smith, E., Landsman, W.B., & Hubeny, I. 2010, ApJ, 718, 1332.
Brown, T.M., Ferguson, H.C., Davidsen, A.F., & Dorman, B.F. 1997, ApJ, 482, 685
Brown, T.M., Smith, E., Ferguson, H.C., Sweigart, A.V, Kimble, R.A, & Bowers, C.W. 2008, ApJ, 682, 319
Brown, T.M., Sweigart, A.V., Lanz, T., Landsman, W.B., & Hubeny, I. 2001, ApJ, 562, 368
Busso, G., et al. 2007, A&A, 474, 105
Cassisi, S., Schlattl, H., Salaris, M., & Weiss, A. 2003, ApJ, 582, L43
Castellani, M., & Castellani, V. 1993, ApJ, 407, 649
Cunha, K., Hubeny, I., & Lanz, T. 2006, ApJ, 647, L143
Dalessandro, E., et al. 2011, MNRAS, 410, 694
D'Antona, F., Bellazzini, M., Caloi, V., Pecci, F.F., Galleti, S., & Rood, R.T. 2005, ApJ, 631, 868
D'Antona, F., Caloi, V., Montalban, J., Ventura, P., & Gratton, R. 2002, A&A, 395, 69
D'Cruz, N.L., Dorman, B., Rood, R.T., & O'Connell, R.W. 1996, ApJ, 466, 359
D'Cruz, N.L., O'Connell, R.W., Rood, R.T., Whitney, J.H., Dorman, B., Landsman, W.B., Hill, R.S., Stecher, T.P., & Bohlin, R.C. 2000, ApJ, 530, 352
Diplas, A., & Savage, B.D. 1994, ApJS, 93, 211
Dotter, A., et al. 2010, ApJ, 708, 698
Fitzpatrick, E.L. 1999, PASP, 111, 63
Fontaine, G., Brassard, P., Green, E.M., Chayer, P., Charpinet, S., Andersen, M., & Portouw, J. 2008, A&A, 486, L39
Gratton, R.G., Carretta, E., Bragaglia, A., Lucatello, S., & D'Orazi, V. 2010, A&A, 517, 81
Grundahl, F., Catelan, M., Landsman, W.B., Stetson, P.B., & Anderson, M.I. 1999, ApJ, 524, 242
Harris, W.E. 1996[8], AJ, 112, 1487
Heber, U. 2009, ARAA, 47, 211
Hu, H., Tout, C.A., Glebbeek, E., & Dupret, M.-A. 2011, MNRAS, in press.
Hubeny, I., & Lanz, T. 1995, ApJ, 439, 875
Lanz, T., Brown, T.M., Sweigart, A.V., Hubeny, I., & Landsman, W.B. 2004, ApJ, 602, 342
Lanz, T., & Hubeny, I. 2003, ApJS, 146, 417
Lanz, T., & Hubeny, I. 2007, ApJS, 169, 83
Miller Bertolami, M.M., Althaus, L.G., Unglaub, K., & Weiss, A. 2008, A&A, 491, 253.
Moehler, S., Dreizler, S., Lanz, T., Bono, G., Sweigart, A.V., Calamida, A., & Nonino, M. 2011, A&A, 526, A136
Pace, G., Recio-Blanco, A., Piotto, G., & Momany, Y. 2006, A&A, 452, 493
Piotto, G., Bedin, L.R., Anderson, J., King, I.R., Cassisi, S., Milone, A.P., Villanova, S., Pietrinferni, A., & Renzini, A. 2007, ApJ, 661, L53
Piotto, G., et al. 2005, ApJ, 621, 777
Randall, S.K., Calamida, A., Fontaine, G., Bono, G., & Brassard, P. 2011, ApJ, 737, L27
Rauch, T., & Ringat, E. 2011, ASPC, 442, 563
Rich, R.M., et al. 1997, ApJ, 474, L25
Rodríguez-Merino, L.H., Chavez, M., Bertone, E., & Buzzoni, A. 2005, ApJ, 626, 411
Servillat, M., et al. 2008, A&A, 641, 654
Sweigart, A.V. 1997, in The Third Conference on Faint Blue Stars, ed. A.G.D. Phillip, J. Liebert, & R.A. Saffer (Schenectady: L. Davis Press), 3

[8] 2010 Edition; Updated at http://physwww.physics.mcmaster.ca/ harris/mwgc.dat